Applied Acoustics 203 (2023) 109227

Contents lists available at ScienceDirect

Applied Acoustics

journal homepage: www.elsevier.com/locate/apacoust

Deep sub-wavelength acoustic transmission enhancement and whisper via the monopole resonance in *meta*-cavities

Yunzhong Lei, Jiu Hui Wu *, Libo Wang, Yao Huang, Jiamin Niu

School of Mechanical Engineering & State Key Laboratory for Strength and Vibration of Mechanical Structures, Xi'an Jiao Tong University, Xi'an 710049, China

ARTICLE INFO

Article history:
Received 9 October 2022
Received in revised form 6 December 2022
Accepted 11 January 2023

Keywords:
Acoustic emission and reception enhancement
Monopole resonance
Private acoustic transmission

ABSTRACT

In this paper, a system consisting of two identical *meta*-cavities that can generate Mie resonances is proposed, aiming to achieve efficient acoustic transmission enhancement and whisper in the deep sub-wavelength range. Unlike traditional Mie resonators with zigzag channels, the *meta*-cavity comprises a central cavity, four straight channels, and eight interconnected side branch cavities. By placing a monopole source in the center or outside of the *meta*-cavity, acoustic emission and reception enhancement can be achieved through monopole resonance, respectively. Considering thermo-viscous loss, The simulation and experimental results show that the acoustic signal detected using the system with the *meta*-cavity radius of 30 mm (0.07λ) is enhanced by 36 dB. While ensuring the same reception, it can reduce the ambient sound pressure level (SPL) by 20 dB to achieve whispering. The system is expected to show significant potential in practical applications based on the results.

1. Introduction

Acoustic transmission enhancement has attracted more and more attention due to its broad application prospects in many acoustic technology fields, such as acoustic communication [1], sonar systems [2], medical imaging, and diagnostics [3]. The radiated sound power of a monopole source is generally low at low frequencies because it is inversely proportional to the square of the wavelength. Due to geometric expansion, the sound pressure amplitude diminishes gradually in free space, severely limiting the strength of the detected signal at the receiver. Therefore, it is necessary to improve the capabilities of acoustic emission and reception. In terms of improving acoustic emission, active devices (speakers) are often used to amplify acoustic signals. The existing problems are that the sizes are on the order of magnitude of the wavelength, the operation is cumbersome, and the SPL of the entire space is improved so that the signal at the receiver has no advantage and is prone to information leakage. Conventional quarter-wave resonators [4] and Helmholtz resonators [5] can be used to improve the ability of acoustic reception. However, the applications at low frequencies are limited by size because the operating frequency is closely related to the length of the structure, and poor robustness is also a complex problem to solve.

In the past few decades, phononic crystals [6–8] and acoustic metamaterials [9–11] have attracted considerable attention because of the acoustic properties that are nearly impossible to achieve in natural materials, such as negative mass density [12], bulk modulus [11], and shear modulus [13], which provide unprecedented opportunities for the development of acoustic transmission enhancement technology. For phononic crystals, Jiang et al. proposed a phononic crystal device with linear defects, which showed ideal acoustic wave directivity at the resonant frequency and realized enhanced directional acoustic sensing characteristics [14]. Wu et al. implemented and modeled acoustic energy harvesting generators based on acoustic wave crystals and piezoelectric materials. Acoustic waves at resonant frequencies can be localized in the cavity of the acoustic wave crystal [15]. However, the existing problem is the large lattice constant at low frequencies. To overcome this shortcoming, small-sized acoustic emission and acoustic receiver devices are realized based on acoustic metamaterials [16–18]. Anisotropic acoustic metamaterials typically rely on resonance effects for acoustic emission and reception enhancement [19,20]. Liu et al. proposed a rigorous analytical model theory to demonstrate that anisotropic acoustic metamaterials can achieve sound multipole emission enhancement [21]. Song et al. proposed a double-walled metamaterial cavity to successfully enhance low-frequency acoustic emission using Fabry-Perot resonance modes [22]. In addition, increasing the equivalent refractive index through spatial folding can compress the sound wavelength and concentrate the sound energy. The sound recep-

* Corresponding author.
E-mail address: ejhwu@xjtu.edu.cn (J. Hui Wu).

https://doi.org/10.1016/j.apacoust.2023.109227
0003-682X/

tion can be enhanced by detecting this significantly amplified pressure field, such as tapered metamaterial waveguides [23,24]. Space-coiling metamaterials with constant and gradient channels [25–28]. Acoustic metasurfaces [29–31], as a class of acoustic metamaterials, can flexibly control the propagation of sound waves by adjusting the phase distribution of the sound field by using generalized Snell's law. Therefore, it can achieve directional emission and acoustic focusing [32–34]. Chen et al. designed an acoustically encoded metasurface lens to achieve broadband tunable focusing in the air [35]. Jahdal et al. fabricated an acoustic lens to focus acoustic waves based on the principle that stacking two materials in different orders and different thicknesses would result in different effective input impedances and refractive indices [36]. Recently, a high relative refractive index labyrinth unit with abundant Mie resonances has attracted interest for a wide range of applications, such as acoustic emission enhancement via the acoustic Purcell effect [37] and directional emission of low-frequency acoustic waves via monopole resonances [38]. Zhang et al. achieved an extraordinary transmission effect with wide tunability from unity to near-zero at low frequencies based on efficient coupling between strong localized sound fields of Mie resonator dimers [39]. Zhang et al. demonstrated efficient non-radiative sound transfer over distances hundreds times longer than the radius of the *meta*-cavities based on the extraordinary scattering characteristics of a pair of eight zigzag channels Mie resonator [40]. Therefore, it inspires us to design a new Mie resonance unit to realize efficient sound transmission enhancement and whisper in the deep sub-wavelength range.

Based on the analysis above, to obtain satisfactory results, a system consisting of two identical *meta*-cavities that can generate Mie resonances is proposed to obtain satisfactory results. The system can achieve high-efficiency acoustic transmission enhancement through the cascade processes of acoustic emission and reception enhancement, which are realized by monopole resonance. Simulation results show that the acoustic transmission can be enhanced by 36 dB compared to free space, and the experimental results verify the simulation conclusion. In addition, the simulation results prove that while ensuring the same reception, the ambient SPL can be reduced by 20 dB to achieve the effect of whispering.

2. Structure design, simulation, and mechanism

In this section, through finite element analysis, it is demonstrated that the proposed *meta*-cavity can realize acoustic emission and reception enhancement, respectively. In addition, the sum of the SPL gains when the *meta*-cavity at the transmitter and receiver exists alone and the SPL gain when the system exists are compared, which aim to observe the process of improving the sound transmission performance of the system more intuitively.

The efficient acoustic transmission enhancement is realized by two identical sub-wavelength *meta*-cavities that can generate Mie resonances, and the schematic illustration established using COMSOL Multiphysics 5.5 is shown in Fig. 1. In theory, a common

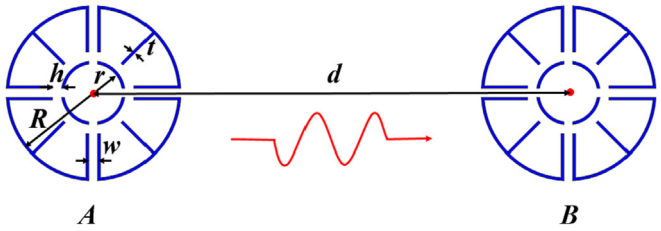

Fig. 1. Schematic illustration of the system composed of two identical *meta*-cavities.

feature of Mie-resonance particles is the high refractive index relative to the background medium. In addition to the zigzag channels, a straight channel with side cavities can achieve a high refractive index [41]. Therefore, the *meta*-cavity consists of a central cavity, four straight channels, and eight interconnected side branch cavities. The inner and outer radii are r = 10 mm and R = 30 mm, respectively. The wall thickness is t = 1 mm, the width of straight channels is w = 3 mm, and the open width of side branch cavities is h = 3 mm. The distance between two *meta*-cavities is d = 1 m. The "Acoustic-Thermo-viscous Acoustic Interaction" module in the finite element software (COMSOL Multiphysics) is used to evaluate the efficient acoustic transmission enhancement performance of the *meta*-cavities. Specifically, the outside of the *meta*-cavities employs the "Pressure Acoustics" module, and the inside is modeled with the "Thermo-viscous Acoustics" module. The frameworks of the *meta*-cavities are set as acoustically rigid. The background air parameters are mass density $\rho = 1.21\ kg/m^3$ and sound velocity c = 343 m/s. A monopole source with a fixed surface velocity $v_0 = 1$ m/s is placed in the center of the *meta*-cavity (subscript A), and the sound is detected in another *meta*-cavity (subscript B) center. Besides, a perfectly matched layer is added to the outermost layer to eliminate the effects of reflections.

Fig. 2 demonstrates the mechanism for improving the acoustic emission and reception efficiencies using the proposed *meta*-cavities, and the system can significantly improve the acoustic transmission efficiency through the cascade processes of acoustic emission and reception enhancements. Where SPL_0, SPL_1, SPL_2, and SPL_3 respectively represent the SPLs of the receiving end in four cases (in the free space, in the presence of *meta*-cavities alone, and simultaneously). $SPL_{1\text{-}0}$, $SPL_{2\text{-}0}$, and $SPL_{3\text{-}0}$ are used as indicators to measure the enhancement of acoustic transmission, representing the SPL gains in the presence of *meta*-cavities alone and simultaneously, respectively. Fig. 2(a) shows the SPL at the receiver in free space.

When the *meta*-cavity is placed at the transmitter, the $SPL_{1\text{-}0}$ measured at the receiver is shown in Fig. 2(b). It can be seen that the enhancement peak appears at 794 Hz, and the $SPL_{1\text{-}0}$ is 18.1 dB, which illustrates that the *meta*-cavity can improve the emissivity of the monopole source. It can be seen from the normalized pressure and phase functions that the enhancement peak at 794 Hz corresponds to the first monopole resonance because of the same acoustic pressure phases in all directions. In acoustic theory, for a monopole source with a given surface velocity U, the radiated sound power P is determined only by the radiation resistance Re(Z) because of $P = U^2Re(Z)/2$. Therefore, the mechanism of the improved acoustic emissivity through the *meta*-cavity is obtained, that is, increasing the radiation resistance of the monopole source through monopole resonance. To verify the above conclusion, the acoustic radiation resistances $Re(Z_1)$ and $Re(Z_0)$ are calculated from the ratio of the acoustic pressure on the surface of the monopole source to the normal velocity, and the results are shown in Fig. 2(c), which show an order of magnitude improvement in radiation resistance in the presence of *meta*-cavity compared to free space. In addition, the peak appeared in $Re(Z_1)$ at 794 Hz, which is consistent with the frequency at the enhanced peak in Fig. 2(b). The simulation results further confirm the mechanism of using the *meta*-cavity to improve acoustic emission efficiency. When the *meta*-cavity is placed at the receiver, the $SPL_{2\text{-}0}$ is shown in Fig. 2(d), the enhancement peak also corresponds to 796 Hz, and the $SPL_{2\text{-}0}$ is 18.1 dB. To analyze the reason for the formation of the enhancement peak, we investigate the pressure and phase functions in the *meta*-cavity at 796 Hz, which show the features of Mie resonance. The equally distributed phase along all directions indicates the generation of the first monopole resonance, which concentrates the acoustic energy in the

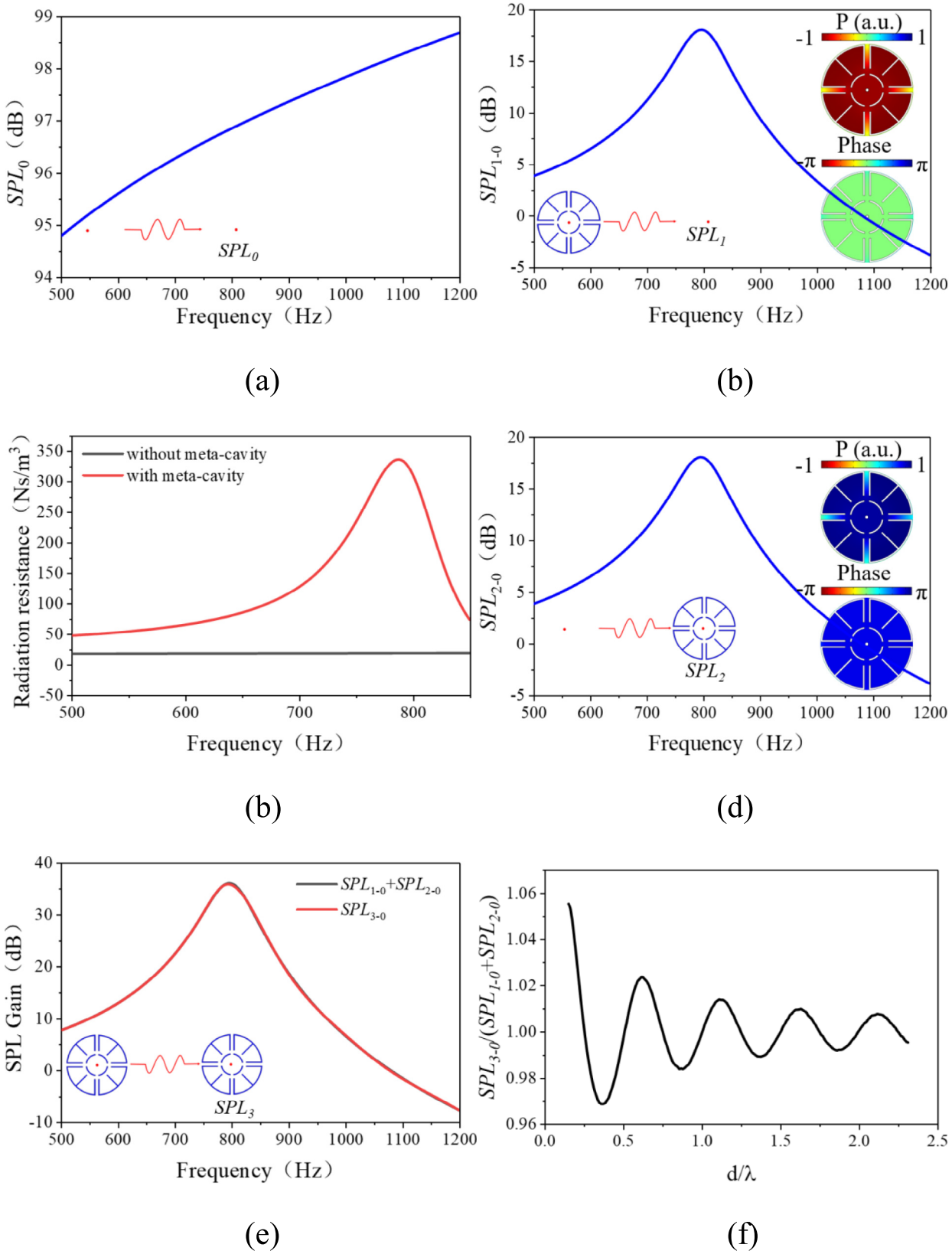

Fig. 2. (a) SPL at receiver in free space. (b) SPL gain in the presence of *meta*-cavity at the transmitter compared to free space. (c) Radiation resistance of the monopole source with or without metamaterial at the transmitter. (d) SPL gain in the presence of *meta*-cavity at the receiver compared to free space. (e) The SPL gain in the presence of the system and the sums of SPL gains in the presence of *meta*-cavities alone. (f) The relationship of $SPL_{3\text{-}0}$ /($SPL_{1\text{-}0}$ + $SPL_{2\text{-}0}$)and d/λ.

meta-cavity. The following conclusion is drawn from the above analysis: Placing the monopole sound source in the center and outside of the *meta*-cavity can achieve acoustic emission and reception enhancement through monopole resonances. In addition, further studies of eigenstates show other resonant modes of the proposed *meta*-cavity (Supplementary Note 1).

Next, to observe the process of improving the sound transmission efficiency of the system more intuitively, we compare the $SPL_{3\text{-}0}$ in the presence of the system and the sums of $SPL_{1\text{-}0}$ and $SPL_{2\text{-}0}$, and the results are plotted in Fig. 2(e), where the red and black curves represent $SPL_{3\text{-}0}$ and $SPL_{1\text{-}0}$ + $SPL_{2\text{-}0}$, respectively, it can be seen that the two curves are almost completely fitted, which shows that the operation of the system can be regarded as the cascaded processes of acoustic emission and acoustic reception.

When the sound wave is incident on the metamaterial at the receiver, scattering will inevitably occur, and the scattered waves generated by different parameters d may have different effects on the SPL gain generated by the system. To avoid the system can only exhibit such performance when the parameter d takes a specific value, in Fig. 2(f), we calculate the relationship between $SPL_{3\text{-}0}$ /($SPL_{1\text{-}0}$ + $SPL_{2\text{-}0}$) and d/λ to evaluate the effect of distance on the cascaded processes. It can be seen that $SPL_{3\text{-}0}$ / ($SPL_{1\text{-}0}$ + $SPL_{2\text{-}0}$) oscillates near 1, but the maximum oscillation amplitude is only 0.06 and becomes smaller as d/λ increases. The result further shows that the cascaded processes are not limited by the distance between the transmitter and the receiver, which can significantly broaden the application field.

3. Effect of the key parameters on the acoustic transmission performance

In this section, the effects of the critical parameters of *meta*-cavity on acoustic transmission performance are investigated thoroughly through finite element simulation, aiming to provide general rules for the design of *meta*-cavity in practical application.

First, the relationship between the parameter h and the SPL gain in the presence of the system is investigated. Fig. 3(a) shows the simulated SPL gain of different m. The black, red, blue, and green lines represent the SPL gain when h = 2 mm, 3 mm, 4 mm, and 5 mm. The other parameters r = 10 mm, T = 1 mm, R = 30 mm and w = 3 mm remain unchanged. It can be seen that with the increase of h, the frequency corresponding to the enhancement peak increases and the peak value gradually decreases. This behavior can be explained from a superficial perspective: the *meta*-cavity can be equivalent to a spring-mass system, where the channel is equivalent to mass, respectively, and the cavity is equivalent to spring with stiffness k. When h increases, the equivalent mass

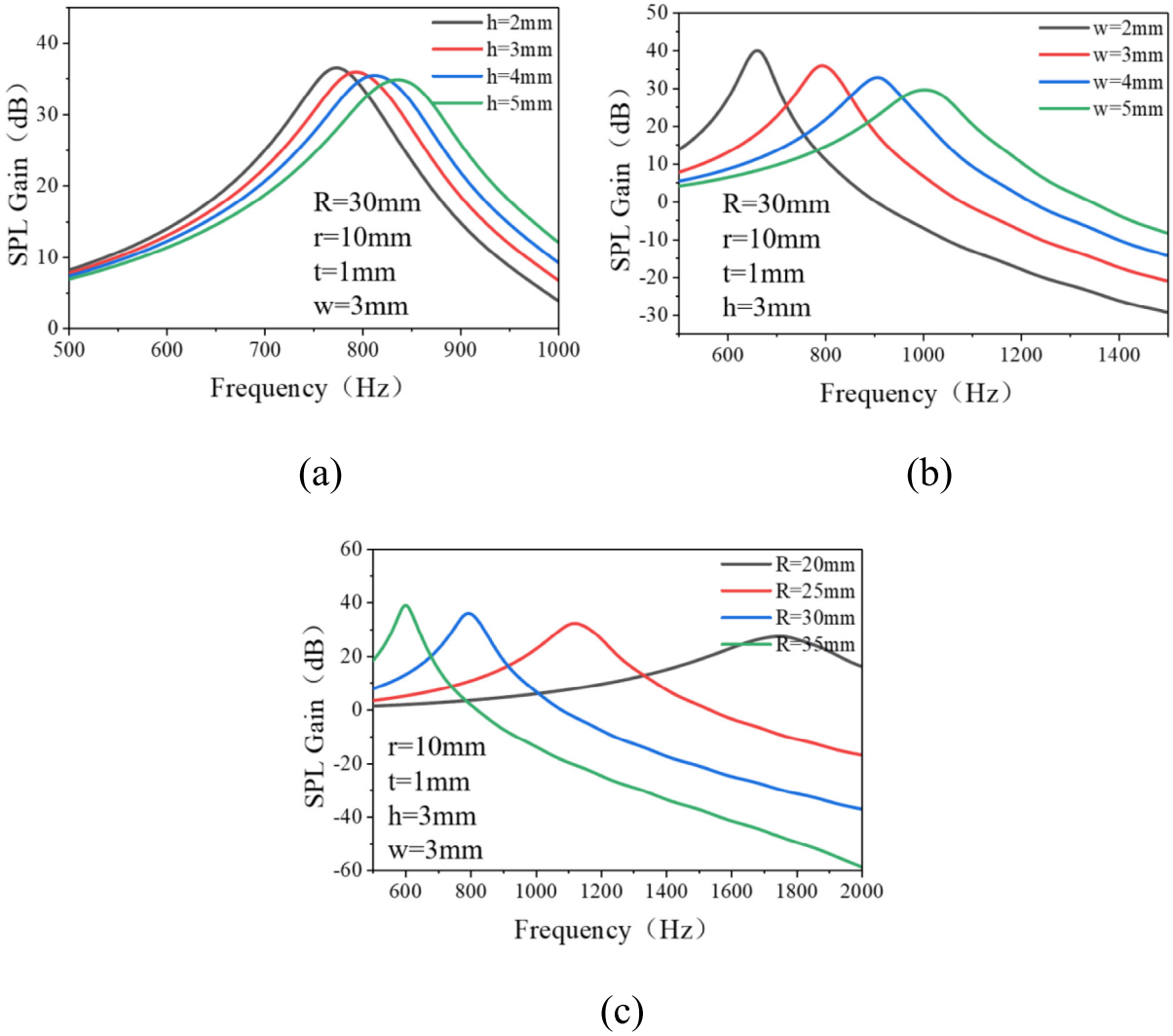

Fig. 3. The relationship between the SPL gain of the system and the parameters h (a), w (b), and R (c).

and quality factor of the system decrease so that the resonant frequency increases and the peak value decreases. Fig. 3(b) shows the SPL gain with different w, where the parameter w is chosen as 2 mm, 3 mm, 4 mm, and 5 mm, and the other parameters r = 10 mm, T = 1 mm, R = 30 mm, and h = 3 mm remain unchanged. It can be found that with the increase of w, the frequency corresponding to the enhancement peak gradually increases, the amplitude of the increase gradually decreases, and the corresponding peak value gradually decreases. The result is also caused by the reduction of the equivalent quality and quality factor of the system.

Fig. 3(c) shows the SPL gain with different R, where the parameter R varies from 20 mm to 35 mm, and the other parameters remain unchanged. Obviously, with the increase of R, the frequency corresponding to the enhancement peak decreases, the magnitude of the decrease decreases, and the corresponding peak value increases. The reasons for the above are that the increased R increases the structure size, and the resonance frequency decreases from the inverse relationship between wavelength and frequency. The above discussion has important guiding significance for choosing appropriate parameters in practical applications.

4. Realization of private transmission of acoustic signals by whisper

In terms of the monopole source, due to the geometric expansion and loss, the sound pressure in the circle with the monopole source as the center and the parameter d as the radius is greater than that at the receiver. Therefore, it is easy to leak during the signal transmission process, and private sound transmission cannot be performed. In this section, we demonstrate the private transmission of acoustic signals through the system by whisper.

The whispering process refers to focusing a highly amplified sound signal from a sound source to a specific location and reducing the sound pressure of the surrounding environment. Next, we will demonstrate how the *meta*-cavities system achieves the process. As shown in Fig. 4(a), in free space, when the fixed surface velocity of the monopole source is v_0 = 1 m/s, the SPL at the receiver at a distance of one meter is 96.8 dB. It can be seen that the SPL within one meter of the transmitter is higher than the receiver, which means we can steal the signal from somewhere else and the result might be better. When we place a sound source with a fixed surface velocity of $v_1 = v_0/61$ at the center of one *meta*-cavity, the SPL we detect at the center of the other *meta*-cavity is

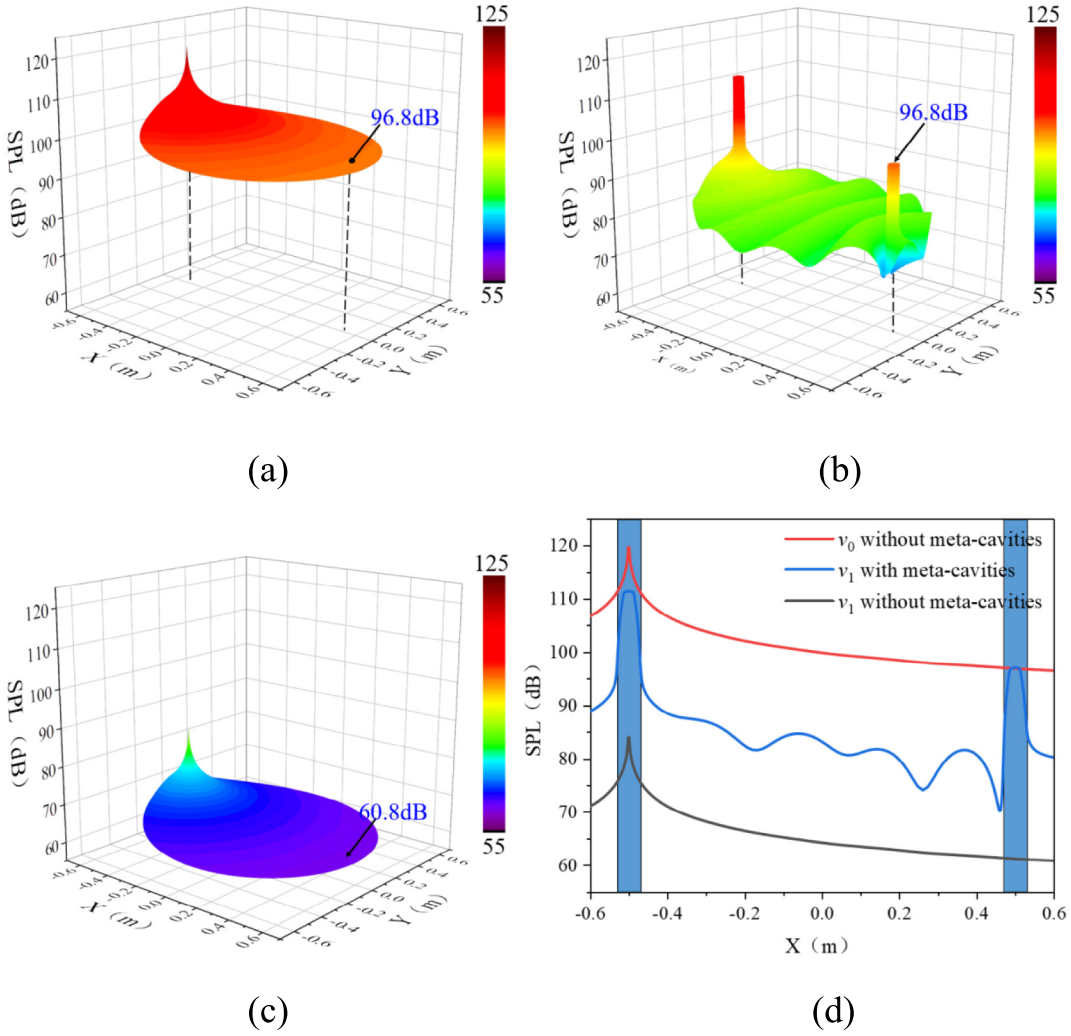

Fig. 4. (a) Sound pressure field in free space when the monopole source has a fixed surface velocity of v_0 = 1 m/s. (b) The sound pressure field in the presence of the system when the monopole source has a fixed surface velocity of $v_1 = v_0/61$. (c) Sound pressure field in free space when the monopole source has a fixed surface velocity of $v_1 = v_0/61$. (d) The SPL along the x-direction when y = 0 in the above three cases.

also 96.8 dB. The result is shown in Fig. 4(b). It can be seen that the SPL in the surrounding space is much lower than that of the transmitter and the receiver so that the signal can be prevented from being stolen while ensuring that the information transmission is not affected. When the sound source with a fixed surface velocity of $v_1 = v_0/61$ is in free space, the SPL at the receiving end is only 60.8 dB, and the result is shown in Fig. 3(c). Next, the SPL profiles of the straight-line path from the transmitter to the receiver are plotted in Fig. 3(d). The red, the blue, and the black lines are respectively the results of the following three cases: a monopole source with a surface velocity of v = 1 m/s in free space, a monopole source with a surface velocity of $v_1 = v_0/61$ in the system, and a monopole source with a surface velocity of $v_1 = v_0/61$ in free space. It can be seen from the red and blue lines that the SPL of the surrounding environment is reduced by an average of 20 dB under the condition that the received signal is not affected, thereby, the concealment of signal transmission is improved, and the signal is prevented from being stolen. It can be seen from the blue and black lines that the SPL at the receiver is increased by 36 dB when the system is present. By comparing with Fig. 2(e), we find that efficient and stable acoustic transmission enhancement can be achieved at a specified location, no matter which monopole source is used.

5. Experiments

In this section, we experimentally measure the SPL gains at the receiver in the presence of *meta*-cavities alone and simultaneously, respectively, and compare it with the simulation results. The high-efficiency acoustic transmission enhancement performance of the system is further verified. The experimental setup is shown in Fig. 5(a). Through 3D printing technology, the *meta*-cavities are precisely fabricated using epoxy resin. Due to the significant acoustic impedance mismatch between the air and epoxy resin,

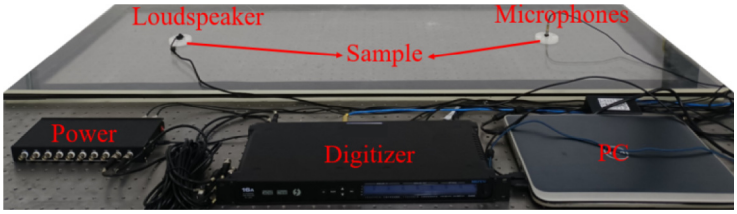

(a)

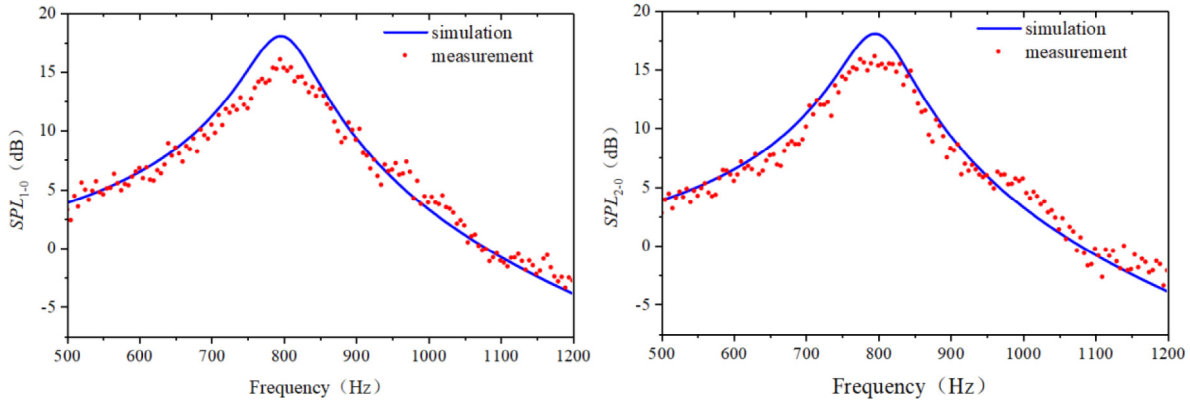

(a) (c)

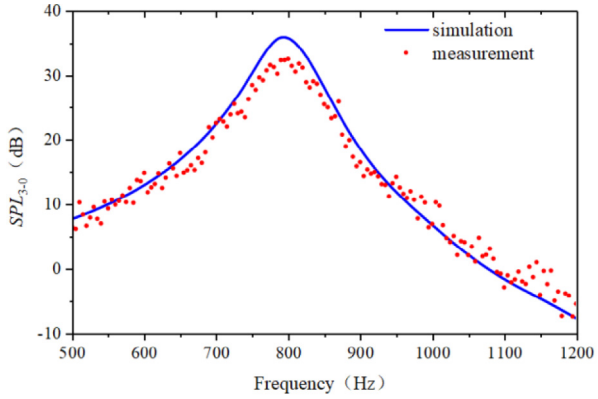

(d)

Fig. 5. (a) Photograph of the experimental setup. (b)-(d) Experimental and simulation measured SPL gain in the presence of *meta*-cavities alone and simultaneously.

the samples can satisfy the hard acoustic field boundary conditions used for the simulation, which are sandwiched between two-dimensional waveguides composed of two parallel acrylic plates. The height of the two experimental samples is 10 mm, and the distance between them is 1 m. The monopole source and microphone are separately placed in the center of the samples and sealed, and the sound-absorbing sponge is placed at the boundary of the waveguide. The sound pressure amplitudes are measured by a digitizer with a frequency range of 500–1200 Hz. The results are shown in Fig. 5(b)-(d), where the blue line and red dot represent the SPL gain obtained by simulation and experiment, respectively. The experimental and simulation results have the same trend, which confirms that placing a monopole source in the center or outside of the *meta*-cavity can achieve acoustic emission and reception enhancement through monopole resonance, respectively. Furthermore, the system is demonstrated to achieve effi-

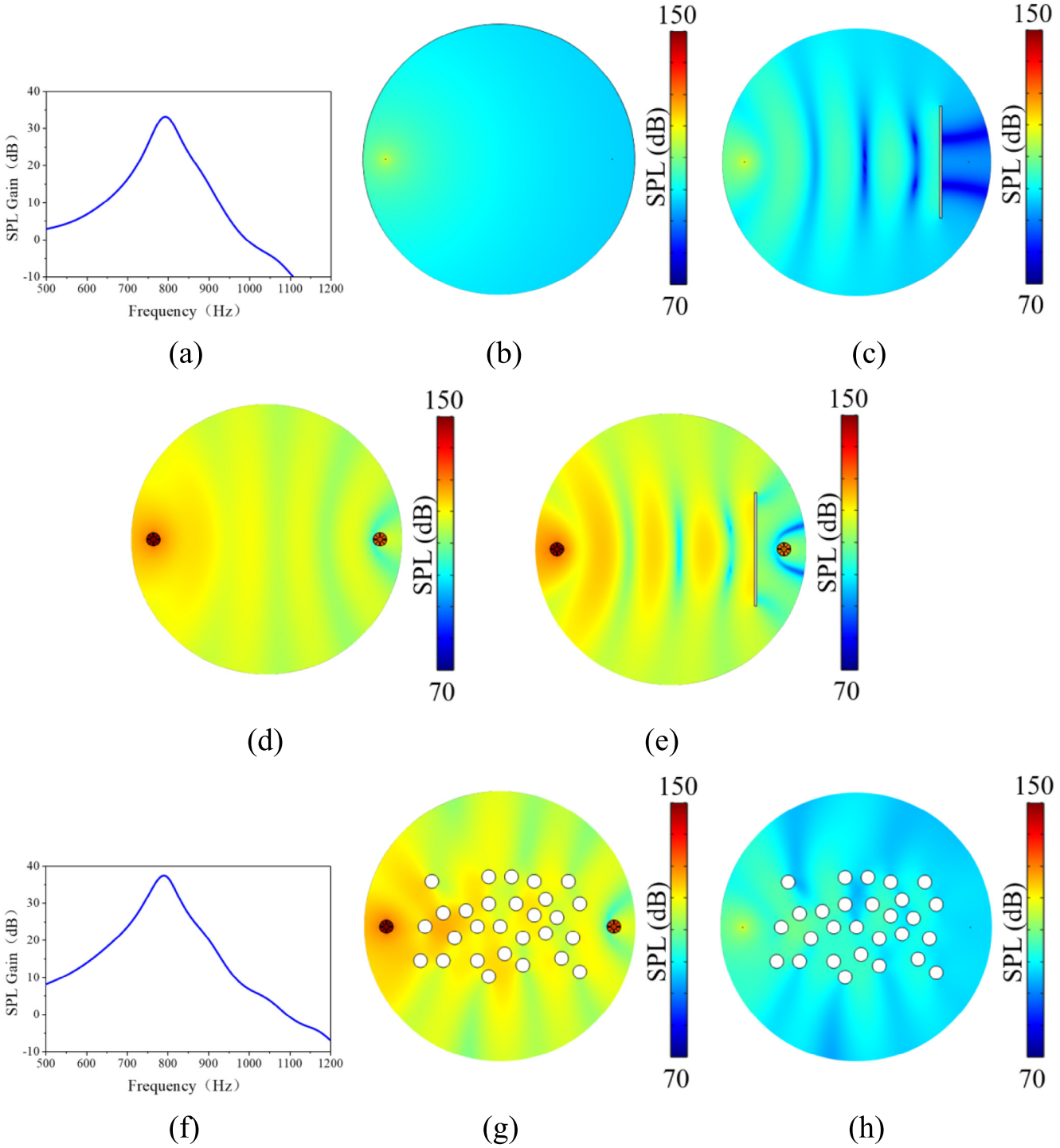

Fig. 6. (a) SPL gain compared to free space at the receiver in the presence of the system and a large obstacle. The sound pressure field at 794 Hz for the following four cases: free space (b), the large obstacle exists (c), the system exists (d), and the large obstacle and system exist simultaneously (e). (f) SPL gain compared to free space at the receiver in the presence of the system and 28 randomly distributed scatterers. The sound pressure field at 794 Hz for the following two cases: the 28 randomly distributed scatterers exist (g), and the 28 randomly distributed scatterers and the system exist simultaneously (h).

cient acoustic transmission enhancement through a cascade process of acoustic emission and reception enhancement. The deviation between the experimentally measured SPL gain and the simulation results can be attributed to the instability of the monopole source and the roughness of the sample surface caused by the 3D printing error.

6. Robustness of the system and extended applications

In this section, a larger obstacle or randomly distributed scatterers are placed between the transmitter and receiver to verify the robustness of the system. Furthermore, we demonstrate the extended applications of the system. Such as placing *meta*-cavities on multiple receivers can enhance multi-target acoustic transmission and underwater acoustic transmission enhancement.

First, we discuss in detail the performance of the system with a large obstacle or randomly distributed scatterers placed between the transmitter and receiver. The results show that the system has good robustness. In the presence of the system, when a large obstacle with a length of 500 mm and a width of 10 mm is placed at a distance of 130 mm from the receiver, the SPL gain of the receiver is plotted in Fig. 6(a). It can be seen that the peak value of the enhancement peak is 33.2 dB, and the corresponding frequency is 794 Hz. In the absence of the obstacle, the peak value of the enhancement peak is 36.0 dB, and the corresponding frequency is 794 Hz. Next, for comparison, we calculated the sound pressure field at 794 Hz for the following four cases: free space, the system and the obstacle exist separately and simultaneously, the results are shown in Fig. 6(b)-(e). It can be found that, compared with the free space, the SPL at the receiver is significantly lower when the obstacle exists alone. Compared with the existence of the system alone, the SPL at the receiver is slightly reduced when the obstacle and the system exist at the same time, but there is a significant gain in the SPL compared with the free space.

In the presence of the system, when 28 scatterers with a radius of 3 mm and an acoustically rigid boundary are randomly placed between the transmitter and receiver, the SPL gain of the receiver is shown in Fig. 6(f). It can be seen that the peak value of the enhancement peak is 37.4 dB, and the corresponding frequency is 790 Hz. Compared to the case without the scatterers, the peak value of the enhancement peak is even higher, and the corresponding frequency is slightly decreased, indicating that the system still has an excellent performance in the very complex sound propagation situation in the presence of the scatterers. The sound pressure field diagrams for the following two cases are plotted in Fig. 6(g)-(h), respectively: the scatterers exist alone, and the scatterers and the system exist simultaneously. In conclusion, the above analysis demonstrates that the system has excellent robustness to various obstacles.

Next, multi-target acoustic transmission enhancement is achieved by placing *meta*-cavities on multiple receivers, and the specific setup is shown in Fig. 7(a). A monopole source with a fixed surface velocity of 1 m/s is placed in the *meta*-cavity (subscript A), and other three *meta*-cavities for the receiver (subscript B-D) are

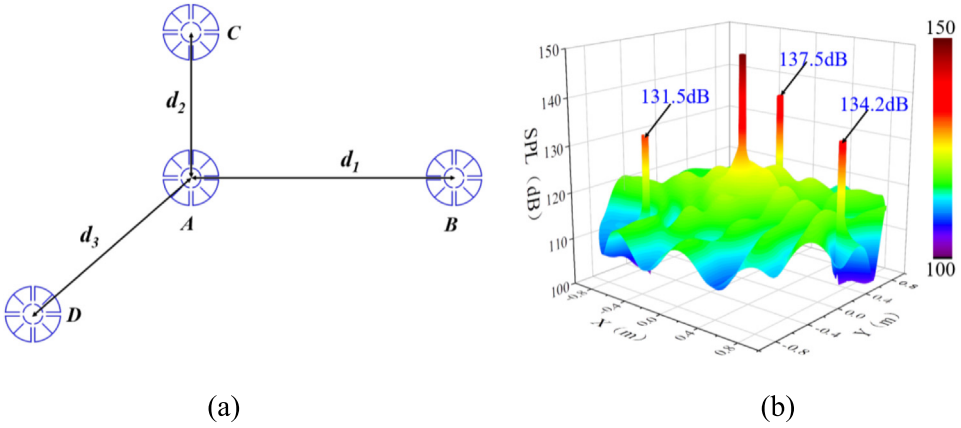

Fig. 7. (a) Schematic illustration of system setup for multi-target acoustic transmission enhancement, where d_1 = 1000 mm, d_2 = 500 mm, d_3 = 800 mm. (b) Sound pressure field in the presence of the system when the monopole source has a fixed surface velocity of v_0 = 1 m/s.

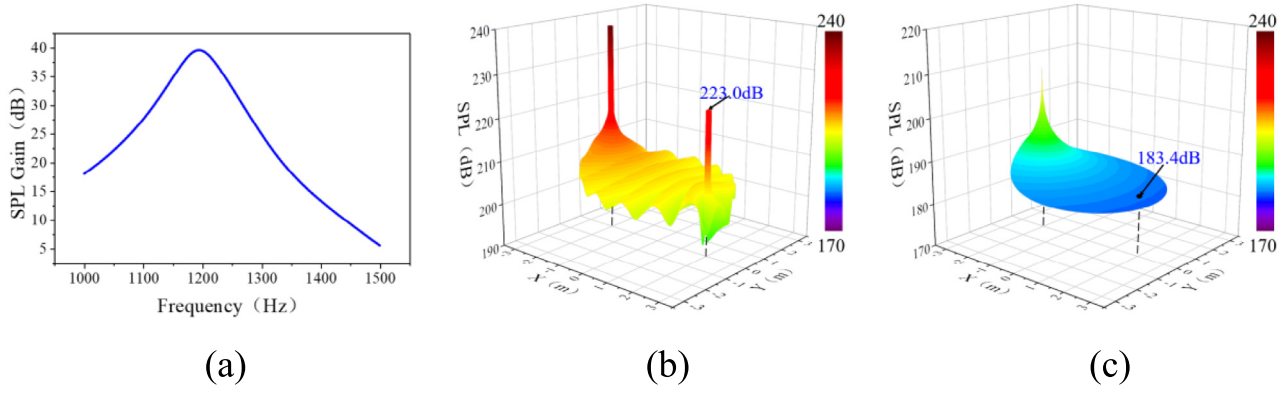

Fig. 8. (a) SPL gain in the presence of the system at the receiver compared to underwater free space. Sound pressure fields in the presence of the system (b) and free space (c), respectively.

scattered around A with the distances of 1000 mm, 500 mm, and 800 mm, respectively. The sound pressure field for multi-target acoustic transmission enhancement is plotted in Fig. 7(b). It can be seen that the SPLs at the three receivers are 134.2 dB, 137.5 dB, and 131.5 dB, which are significantly higher than that at other surrounding locations. The results show that acoustic transmission enhancement can be realized at multiple specified locations by placing *meta*-cavities on multiple receivers.

Finally, the underwater high-efficiency acoustic transmission enhancement is investigated by full-wave numerical simulation. To avoid thin-wall vibration, the parameters of the *meta*-cavity are set as R = 100 mm, r = 20 mm, d = 4 m, and t = w = h = 10 m m. The simulation results are shown in Fig. 8(a). It can be seen that the frequency corresponding to the enhancement peak is 1194 Hz, and the SPL gain is 39.6 dB. The sound pressure fields are plotted in Fig. 8(b)-(c) for the following two cases: in free space and the presence of the system. It can be seen that in free space, the SPL of the receiver is 183.4 dB and the sound pressure within 4 m of the transmitter is higher than that of the receiver. However, when the system exists, the SPL at the receiver is 223.0 dB, and the sound pressure in the surrounding space is much lower than that of the transmitter and receiver. The above analysis shows that the system can still be used for efficient sound transmission enhancement and whisper underwater. Moreover, we further demonstrate the excellent performance of the proposed system by comparing it with classic Helmholtz resonators (Supplementary Note 2).

7. Conclusion

In conclusion, a system consisting of two identical *meta*-cavities is proposed to achieve efficient sound transmission enhancement and whisper. The *meta*-cavity is composed of a central cavity, four straight channels, and eight interconnected side branch cavities, which can improve the radiation resistance by changing the external environment of the monopole source through monopole resonance to achieve acoustic emission enhancement. In addition, acoustic reception enhancement can be achieved by concentrating acoustic energy through monopole resonance. The system can achieve high-efficiency acoustic transmission enhancement through the cascade processes of acoustic emission and reception enhancement. The dependence of acoustic transmission enhancement on the *meta*-cavity parameters is investigated thoroughly. By increasing h and w and decreasing R, the frequency corresponding to the enhancement peak gradually increases, and the corresponding peak value gradually decreases. The simulation and experimental results show that compared with free space, the sound transmission can be enhanced by up to 36 dB, and we can also perform multi-target acoustic transmission enhancement. In addition, the simulation results prove that the ambient SPL can be reduced by 20 dB under the condition of ensuring the same reception to achieve whispering. Moreover, the filling rate (14.4 %) of the proposed *meta*-cavity is much lower than that of conventional zigzag channels Mie resonator. The study provides new guidance for the realization of acoustic transmission enhancement and whispering. The system has good robustness and great potential for practical applications, such as the detection of weak signals and underwater long-distance acoustic communication.

CRediT authorship contribution statement

Yunzhong Lei: Conceptualization, Methodology, Software, Validation, Writing – original draft, Writing – review & editing. **Jiu Hui Wu:** Writing – review & editing. **Libo Wang:** Writing – review & editing. **Yao Huang:** Validation. **Jiamin Niu:** Validation.

Data availability

Data will be made available on request.

Declaration of Competing Interest

The authors declare that they have no known competing financial interests or personal relationships that could have appeared to influence the work reported in this paper.

Acknowledgement

We acknowledge financial support of the National Natural Science Foundation of China (Nos. 51675401).

Appendix A. Supplementary data

Supplementary data to this article can be found online at https://doi.org/10.1016/j.apacoust.2023.109227.

References

[1] Zhiwang Z, Ye T, Yihe W, et al. Directional acoustic antennas based on valley-hall topological insulators. Adv Mater 2018.
[2] Josserand T, Wolley J. A miniature high resolution 3-D imaging sonar. Ultrasonics 2011;51:275.
[3] Bucci OM, Crocco L, Scapaticci R, Bellizzi G. On the Design of Phased Arrays for Medical Applications. Proceedings of the IEEE. 2016;104:633-48.
[4] Li B, You JH, Kim Y-J. Low frequency acoustic energy harvesting using PZT piezoelectric plates in a straight tube resonator. Smart Mater Struct 2013;22.
[5] Liu F, Phipps A, Horowitz S, Ngo K, Cattafesta L, Nishida T, et al. Acoustic energy harvesting using an electromechanical Helmholtz resonator. J Acoust Soc Am 2008;123:1983–90.
[6] Yang S, Page JH, Liu Z, Cowan ML, Chan CT, Sheng P. Focusing of sound in a 3D phononic crystal. Phys Rev Lett 2004;93:024301.
[7] Lu J, Qiu C, Ke M, Liu Z. Valley vortex states in sonic crystals. Phys Rev Lett 2016;116:093901.
[8] Wu TT, Huang ZG, Lin S. Surface and bulk acoustic waves in two-dimensional phononic crystal consisting of materials with general anisotropy. Phys Rev B 2004:69.
[9] Yang Z, Mei J, Yang M, Chan NH, Sheng P. Membrane-type acoustic metamaterial with negative dynamic mass. Phys Rev Lett 2008;101:204301.
[10] Li J, Chan CT. Double-negative acoustic metamaterial. Phys Rev E 2004;70:055602.
[11] Fang N, Xi D, Xu J, Ambati M, Srituravanich W, Sun C, et al. Ultrasonic metamaterials with negative modulus. Nat Mater 2006;5:452–6.
[12] Liu Z, Zhang X, Mao Y, Zhu YY, Yang Z, Chan CT, et al. Locally resonant sonic materials. Science 2000;289.
[13] Lai Y, Wu Y, Sheng P, Zhang ZQ. Hybrid elastic solids. Nat Mater 2011;10.
[14] Jiang T, He Q, Peng ZK. Enhanced directional acoustic sensing with phononic crystal cavity resonance. Appl Phys Lett 2018;112.
[15] Wu LY, Chen LW, Liu CM. Acoustic energy harvesting using resonant cavity of a sonic crystal. Appl Phys Lett 2009;95.
[16] Zhang S, Yin L, Fang N. Focusing ultrasound with an acoustic metamaterial network. Phys Rev Lett 2009;102:194301.
[17] Wang W, Xie Y, Konneker A, Popa BI, Cummer SA. Design and demonstration of broadband thin planar diffractive acoustic lenses. Appl Phys Lett 2014;105.
[18] Naify CJ, Rogers JS, Guild MD, Rohde CA, Orris GJ. Evaluation of the resolution of a metamaterial acoustic leaky wave antenna. J Acoust Soc Am 2016;139:3251.
[19] Lei Y, Huang Z, Yang S. Enhanced broadband monopole emission and acoustic energy harvesting via a dual anisotropic metamaterial. J Phys D Appl Phys 2022;55:065301.
[20] Qian J, Sun H-x, Yuan S-q, Liu X-j. Enhanced directional acoustic emission based on anisotropic metamaterials. Appl Phys Lett 2019:114.
[21] Liu F, Li W, Ke M. Rigorous analytical model for multipole emission enhancement using acoustic metamaterials. Phys Rev Appl 2018:10.
[22] Song K, Lee SH, Kim K, Hur S, Kim J. Emission enhancement of sound emitters using an acoustic metamaterial cavity. Sci Rep 2014:4.
[23] Chen Y, Liu H, Reilly M, Bae H, Yu M. Enhanced acoustic sensing through wave compression and pressure amplification in anisotropic metamaterials. Nat Commun 2014;5:5247.
[24] Jiang X, Liang B, Li R-q, Zou X-y, Yin L-l, Cheng J-c. Ultra-broadband absorption by acoustic metamaterials. Appl Phys Lett 2014:105.
[25] Li Y, Liang B, Zou X-y, Cheng J-c. Extraordinary acoustic transmission through ultrathin acoustic metamaterials by coiling up space. Appl Phys Lett 2013:103.
[26] Li Y, Liang B, Tao X, Zhu X-f, Zou X-y, Cheng J-c. Acoustic focusing by coiling up space. Appl Phys Lett 2012:101.

[27] Tong S, Ren C, Tang W. Broadband extraordinary acoustic transmission via hornlike metamaterials. Appl Phys Express 2018;11.
[28] Tang W, Ren C, Tong S, Zhou Z. Broadband acoustic transmission enhancement through metamaterials with gradual-type channels. Appl Phys Express 2018;11.
[29] Ma G, Yang M, Xiao S, Yang Z, Sheng P. Acoustic metasurface with hybrid resonances. Nat Mater 2014;13:873–8.
[30] Li Y, Shen C, Xie Y, Li J, Wang W, Cummer SA, et al. Tunable asymmetric transmission via lossy acoustic metasurfaces. Phys Rev Lett 2017;119:035501.
[31] Yong L, Assouar BM. Acoustic metasurface-based perfect absorber with deep subwavelength thickness. Appl Phys Lett 2016;108:204301.
[32] Xia J-p, Zhang X-t, Sun H-x, Yuan S-q, Qian J, Ge Y. Broadband tunable acoustic asymmetric focusing lens from dual-layer metasurfaces. Phys Rev Appl 2018:10.
[33] Fan S-W, Zhao S-D, Cao L, Zhu Y, Chen AL, Wang Y-F, et al. Reconfigurable curved metasurface for acoustic cloaking and illusion. Phys Rev B 2020:101.
[34] Qi S, Li Y, Assouar B. Acoustic focusing and energy confinement based on multilateral metasurfaces. Phys Rev Appl 2017:7.
[35] Chen D-C, Zhu X-F, Wei Q, Yao J, Wu D-J. Broadband tunable focusing lenses by acoustic coding metasurfaces. J Phys D Appl Phys 2020:53.
[36] Al Jahdali R, Wu Y. High transmission acoustic focusing by impedance-matched acoustic meta-surfaces. Appl Phys Lett 2016;108.
[37] Landi M, Zhao J, Prather WE, Wu Y, Zhang L. Acoustic Purcell effect for enhanced emission. Phys Rev Lett 2018;120:114301.
[38] Gengxi Lu, Erliang D, Yangyang W, et al. Realization of acoustic wave directivity at low frequencies with a subwavelength Mie resonant structure. Appl Phys Lett 2017;110:123507 -.
[39] Zhang J, Cheng Y, Liu X. Extraordinary acoustic transmission at low frequency by a tunable acoustic impedance metasurface based on coupled Mie resonators. Appl Phys Lett 2017;110.
[40] Zhang J, Rui W, Ma C, Cheng Y, Liu X, Christensen J. Remote whispering metamaterial for non-radiative transceiving of ultra-weak sound. Nat Commun 2021;12:3670.
[41] Ma F, Zhang H, Du P, Wang C, Wu JH. An underwater planar lens for broadband acoustic concentrator. Appl Phys Lett 2022;120.